Design of the New MST Radar in Chinese Meridian Project

Gang Chen, Zhiqiu He, Shaodong Zhang, Brian Fuller, Wanlin Gong, Guotao Yang, and Weifan Zhang

***Abstract*—With the support of the second phase of the Chinese Meridian Project, a new mesosphere–stratosphere–troposphere observation radar (MST radar), called Qinzhou MST radar, located in Qinzhou City, Guangxi Province, China (22°7′55″N,108°16′20″E) is under construction. The Qinzhou MST radar is a large VHF monostatic pulse Doppler radar with an active phased array antenna system, mainly using Doppler beam swinging technique for observation. The capability of multibeam observation, space antenna observation, and frequency- and spatial-domain interferometry are also employed. The main scientific objective of this radar is to explore the atmosphere dynamical processes at low latitudes of China. The observation of ionospheric field-aligned irregularities (FAIs) is also an important function of the radar. The radar applies a circular array composed of 1261 3-element crossed Yagi antennas with a diameter of 153 m and an aperture of near 2×10^4 m^2. Thereinto, 997 elements connect both transmitting and receiving channels and 264 elements distributed near the edge connect only receiving channels. The peak power of the transmitter in each transmitting/receiving (T/R) module is 2 kW. The central frequency and bandwidth of the output signal are 50 and 4 MHz, respectively. The peak power of the whole system will be close to 2 MW. This article presents the initial design of the Qinzhou MST radar, and the construction will be completed at the end of 2022.**

***Index Terms*—Antenna array, atmosphere observation, mesosphere–stratosphere–troposphere observation radar (MST radar).**

I. Introduction

MESOSPHERE–STRATOSPHERE–TROPOSPHERE observation radar (MST radar) is a kind of wind profiling radar and can detect the echoes from mesosphere, stratosphere, and troposphere. The radar with lower performance that can only record the stratospheric and tropospheric echoes is called an ST radar. The main echoes of the radio systems are scattered from turbulent irregularities (Bragg scattering) or reflected from horizontally stratified structures (Fresnel reflection). At the altitude of upper mesosphere, the meteor scatter and thermal (or Thomson) scatter play a dominant role for the echoes [1]–[3]. An MST radar is primarily used to observe the atmospheric wind fields and turbulence at the stratospheric heights up to 25 km as well as the mesospheric region from 55 to 85 km, and able to study the coupling and some interesting phenomenon between atmospheric layers [5], [22]–[31]. Some MST radars also have the ability to observe the ionospheric electron density and FAIs [32]–[39]. The theoretical foundations for MST/ST radar were established as early as the 1950s [4]. Before long, the first MST radar in the world, the Jicamarca radar, was built in Peru in 1961 [5]. In the 1970s, other MST radars that operated in VHF band emerged in succession, including the SOUSY radar in Germany, the Poker Flat radar in Alaska, and the Sunset radar and the Platteville radar in Colorado [1], [6]–[10]. After that, more MST radars were built in Asia. In the east of Asia, an observation chain of MST radars distributes from 34.85° N to 0.2° S latitudes. The middle and upper atmosphere (MU) radar at Shigaraki, Shiga, Japan, and the equatorial atmosphere radar (EAR) at the equator near Bukittinggi, West Sumatra, Indonesia, locate in the north and south ends of the chain [11]–[13]. The Beijing and Wuhan MST radars, as well as the Chung-Li VHF radar situate in the middle of the chain [14], [15]. In South Asia, the Gadanki radar is located near the geomagnetic equator [18]. Moreover, the Resolute Bay VHF radar applying a cross-shaped antenna array was established in Nunavut, Canada, and the MAARSY is operated on the North-Norwegian island of Andøya [19], [20]. In early 2011, the first MST radar in Antarctica—the PANSY radar—was installed [21].

Supported by the first phase of the Chinese Meridian Space Weather Monitoring Project (Meridian Project) [40], [41], we have established three VHF radars, two of which are MST radars. The two MST radars have been installed in Beijing and Wuhan, China, for long-term continuous operation [14] and they are required to work for more than 6720 h every year. The other VHF radar, the HCOPAR located at low latitude is a coherent scatter radar for ionospheric irregularity observation [46]. Readers can access their data freely from the Meridian Project data center.[1] In the past years, the two MST radars have recorded abundant atmospheric echoes, including the mesospheric echoes and achieved the expected target [24], [42]. Supported by the second phase of Chinese Meridian Project, a new powerful and functional MST radar with high reliability and expansibility is

Manuscript received November 5, 2020; revised January 5, 2021; accepted January 23, 2021. Date of publication February 8, 2021; date of current version March 5, 2021. This work was supported in part by the Chinese Meridian Project and in part by the National Natural Science Foundation of China under Grant 41722404. *(Corresponding author: Gang Chen.)*

Gang Chen, Zhiqiu He, Shaodong Zhang, Wanlin Gong, and Weifan Zhang are with the Electronic Information School, Wuhan University, Wuhan 430072, China (e-mail: g.chen@whu.edu.cn; zqhe1234@whu.edu.cn; zsd@whu.edu.cn; gongwl@whu.edu.cn; zhangweifan@whu.edu.cn).

Brian Fuller is with the Genesis Software, Pty Ltd., Adelaide, SA 077190, Australia (e-mail: bfuller@gsoft.com.au).

Guotao Yang is with the National Space Science Center, Chinese Academy of Sciences, Beijing 100864, China (e-mail: gtyang@spaceweather.ac.cn).

Digital Object Identifier 10.1109/JSTARS.2021.3057610

[1][Online]. Available: https://data.meridianproject.ac.cn/

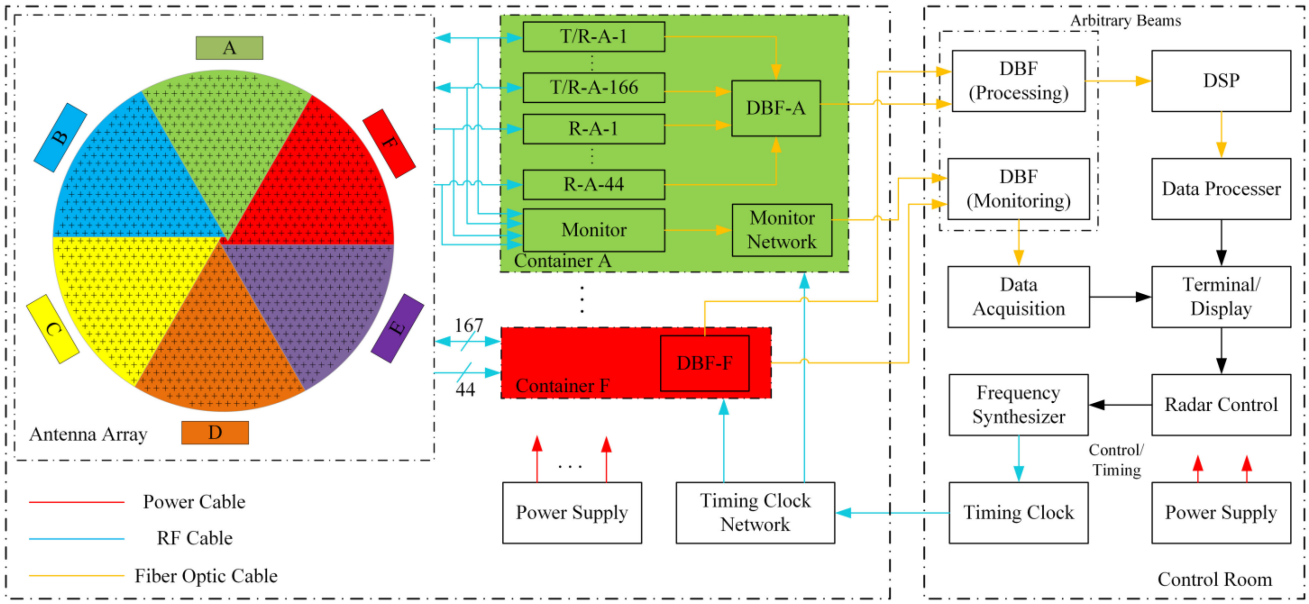

Fig. 1. System block diagram of the Qinzhou MST radar.

under construction. This article introduces the design of the new MST radar. The overall design of the radar is presented in Section II, the outdoor antenna array system is discussed in Section III, the indoor hardware system is introduced in Section IV, and Section V draws the conclusion of the whole radio system and introduces the construction period of the radar.

II. Overall Design of the Radar

In the first phase of the Chinese Meridian Project, two MST radars were located in middle latitudes. In the second phase, we plan to build a new MST radar in the low latitude of China. After years of investigation and evaluation, the construction site is selected at Qinzhou, Guangxi province, China (22°7′55″N,108°16′20″E), eventually and the new radar will be named as Qinzhou MST radar. The basic mission of the new radar is to observe the low-latitude 3-D winds in the troposphere, stratosphere, and mesosphere, study the coupling between different neutral layers, between neutral atmosphere and ionosphere, as well as investigate the latitudinal dependency of atmospheric structure and wave propagation, accompanying the observations of the Beijing and Wuhan MST radars. Apart from the basic mission, the new radar is also required to possess the following capabilities.

1) Observation of E and F-region FAIs.
2) Spatial-domain interferometry observation [49].
3) Frequency-domain interferometry (FDI) [45], [58] and frequency-domain interferometric imaging (FII) [60].
4) Spaced antenna observation mode [59] and multibeam observation mode [19].
5) Meteor mode [19] [61].

An overall blueprint of the Qinzhou MST radar is designed by multi-institutional collaborations and it is currently in the construction phase. The system block diagram of the Qinzhou MST radar is presented in Fig. 1 and the basic parameters are listed in Table I. The Qinzhou MST radar will be the first full element level digital array radar among all existing MST radars, and an active circular array with 1261 regularly distributed antennas is adopted. There are 997 transmitting and 1261 receiving channels at most. Each digital transmitting channel equips a completely independent controllable digital T/R module with highly precise

TABLE I
Basic Parameters of the Qinzhou MST Radar

Parameter	Specification
location	(22°7'55" N, 108°16'20" E), near Qinzhou, Guangxi province, China
radar system	monostatic pulse coded radar with an active circular phased array
allocated bandwidth	4 MHz
operating frequency	50 MHz (49 MHz-51 MHz)
peak power	~ 2 MW (maximum), each transmitting power is selectable in 0.5, 1 and 2 kW
duty cycle	≤ 10 %
chip width	≥ 0.33 μs
APAP	~ 3×10^{10} Wm^2
antenna	
antenna spacing	4.2 m (0.7λ)
aperture	near 2×10^4 m^2 with 153 m in diameter
antenna array	circular thinned array of 1261 3- element crossed Yagi antennas with 997 elements transmitting
HPBW (TX beam)	3° for zenith = 0° 3.5° for zenith = 35°
maximum gain	36.66 dB for zenith = 0° 35.2 dB for zenith = 35°
beam directions	arbitrary at zenith < 35°
VSWR	< 1.2
transmitting channel	997 (at most)
receiving channel	1261 (at most)
waveform	single pulse, Barker and complementary codes, etc.

phase control and scalable radiation power up to 2 kW, and the peak power of the whole system is near 2 MW. Six containers are distributed around the edge of the antenna array and contain all active components. Fast beam steer is available and thousands of radiation directions can be steered per second within an off-zenith angle of 35°. Barker and complementary codes will be primarily adopted for pulse compression without compromising the range resolution [13]. Each T/R module is equipped with an independent direct digital synthesizer (DDS). The RF signals are generated by the DDS and radiated to the space after multilevel amplifying. The received signals are directly sampled in each receiving channel after multilevel amplifying and filtering. The I/Q signals of 1261 channels can be weighted at will and combined in digital beam forming (DBF) subsystem to form the expected receiving beams, which are later sent to digital signal processing (DSP) subsystem and data processing (DP) subsystem to generate product data. The radiation power of each T/R module is monitored by the monitoring subsystem and the integrated frequency subsystem provides the reference clock to the whole system. All the operations are controlled by the display/control subsystem on a pulse-to-pulse basis. Several subsystems are discussed in detail in the following sections.

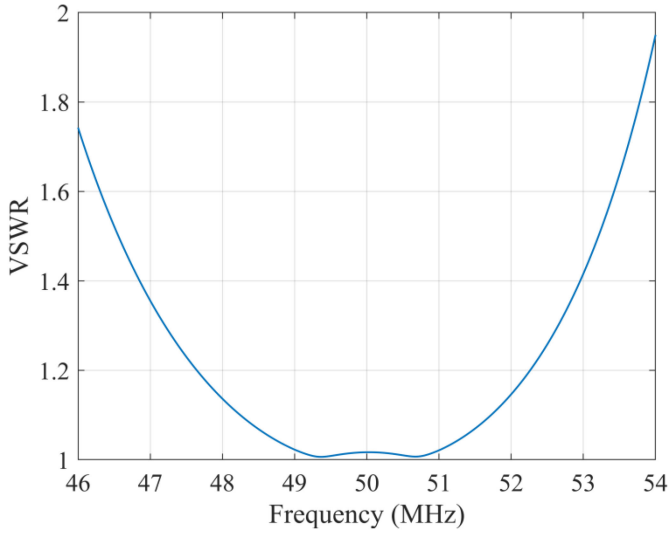

Fig. 2. VSWR versus frequency plot of the 3-element Yagi antenna. The VSWR is below 1.2 within the frequency band between 48–52 MHz.

III. Antenna

A. Antenna Unit

The Qinzhou MST radar uses 3-element Yagi antennas for the excellent directivity. The antenna is designed by the Computer Simulation Technology MICROWAVE STUDIO (CST MWS) software based on the trust region framework to find the optimal solution with relatively large gain and low voltage standing wave ratio (VSWR) within at least 4 MHz frequency band centered at 50 MHz. The 50-MHz operating frequency is suggested by the local electromagnetic environment and terrain. The VSWR is required to be less than 1.2 within the specified frequency band. Fig. 2 shows the VSWR of the Yagi antenna. The VSWR is lower than 1.2 within the frequency band between 48– 52 MHz. The numerical simulated gain of the Yagi antenna is 7 dB and the HPBW is 80°.

B. Antenna Array Design

There are a variety of solutions in designing an MST radar antenna array. The MU radar, EAR, and MAARSY arrange the antennas in a circular array with a uniform equilateral triangular grid [11], [13], [19]. In a large number of cases (e.g., [14], [18]), the antennas are arranged in a square array with a uniform rectangular grid. The antennas in mobile SOUSY and the Resolute Bay radar are gathered into a number of equifed clusters [8], [20]. Moreover, for special purpose, the Resolute Bay radar uses a cross-shaped array to produce a narrow main lobe with relatively less antenna number [20], [50]. The Chung-Li MST radar uses a T-shaped array for spaced antenna and FDI experiment [15], [58]. The Qinzhou MST radar will adopt a circular array with the antenna elements arranged in an equilateral triangular grid. The radius of the circular array is near 13λ. Due to the circular array, the 3-D radiation pattern of the vertical beam of the antenna array is vertical-axisymmetric. The triangular grid allows the array to generate a larger zenith angle free from grating lobes. Fig. 3 displays one optimized amplitude distribution of the Qinzhou MST radar antenna array, wherein each symbol represents an antenna. The colorful cross symbols represent the antennas connecting transmitters and

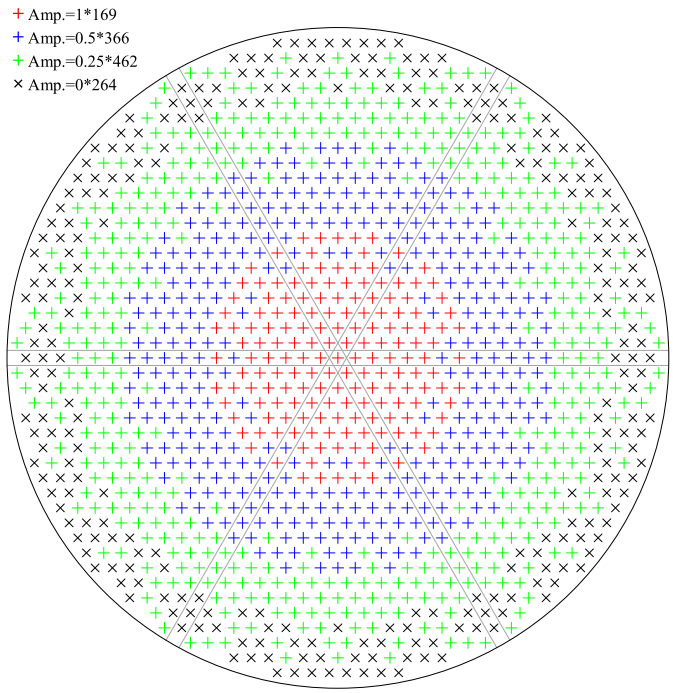

Fig. 3. Sketch of the Qinzhou MST radar antenna array. Each symbol represents a crossed Yagi antenna. Different symbols denote the different illumination amplitudes. The transmitting power of the antennas represented by red, blue, and green crosses can be adjusted among 0.5, 1, and 2 kW. The amplitude distribution displayed here is one kind of optimized distribution. The black oblique cross symbols denote that the corresponding antennas are with no output power on transmission.

the black oblique cross symbols denote the antennas without output power, but only connecting receiving channels. There are 169 antennas transmitting full power (red crosses), 366 antennas transmitting half-power (blue crosses), 462 antennas transmitting quarter-power (green crosses), and 264 antennas having no transmitting power (oblique black crosses). Except the antennas having no transmitting power, the transmitting power of the remaining antennas can be adjusted among 0.5, 1, and 2 kW.

The antenna spacing d selected here is the maximum value without grating lobes, even when the radiation beam tilts to 35° off-zenith at any azimuth. The maximum off-zenith angle of the antenna array is chosen according to the local magnetic inclination. The array is required to form the beams vertical to the local geomagnetic fields for ionospheric FAIs observations. A smaller antenna spacing will increase the antenna coupling.

The movement of the grating lobes can be effectively estimated in a complex T plane, where $T = u + jv$, $u = \sin\theta\,\cos\phi$, and $v = \sin\theta\,\sin\phi$. In this plane, the part within the unit circle is called as "$\sin\theta$- space" or "real space," representing the projection of the unit sphere on the plane of the array. The outside part is unobservable and called as "imaginary space" [16]. Normally, the grating lobes situate in the "imaginary space," but can move into the "real space" along with the deflection of the radiation beam. The optimal spacing d can be attained by analyzing the movement of the grating lobes. Referring to the method introduced in [17], the maximum attainable zenith angle $\theta_{\max}$ has the minimum value when the azimuth is 30° within the azimuth range of (0°, 90°). While selecting the antenna spacing, we should guarantee that no grating lobe appears when the zenith angle tilts to 35° at the azimuth of 30°. After several attempts, the antenna spacing d is finally determined as 0.7λ. Fig. 4 shows the sketch of the utmost scan coverage of the antenna array and the details are introduced in the caption. It is evident that when the zenith angle tilts to 35° at the azimuth of 30°, the entire grating lobe is just outside the "real space".

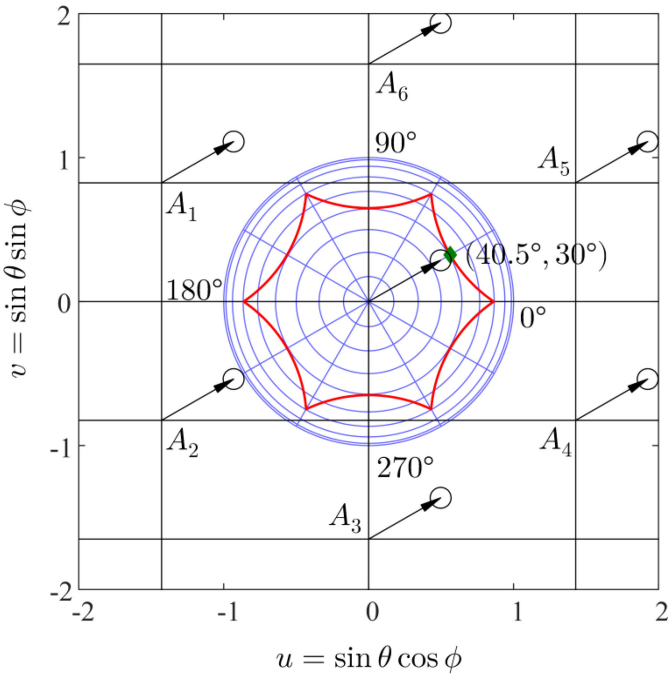

Fig. 4. Sketch of utmost scan coverage of the Qinzhou MST radar antenna array in complex T plane. A_1–A_6 are the sites of the grating lobes with the most potential to move into the "real space" within the maximum blue circle. The blue circle is drawn every 10°. The small black arrows provide the radiation direction ($\theta_{\max}$, $\phi_{\max}$) of the beam. The angle between the arrow and the u-axis is $\phi_{\max}$ and the length of the arrow is $\sin\theta_{\max}$. The small black circles represent the profiles of the first null lines of both the grating lobes and the main lobe. The thick red curve is the utmost scan coverage when the main lobe or grating lobes is regarded as a point in T plane, and the actual scan coverage is slightly smaller. The interval between two adjacent vertical black lines is λ/d_x and the interval between two adjacent horizontal black lines is λ/d_y, where $d_x = d$, $d_y = \sqrt{3}\,d$.

C. Antenna Array Pattern

Uniform weighting is commonly used in MST radar antenna array. However, an array with uniform weighting will generate high sidelobe level (SLL), which often leads to the misjudgment of the echo direction. MST radars are often required to operate with high power for a long time. It is not realistic to add any attenuators to control the amplitude weighting. Currently, some equivalent approaches are developed and can achieve the desired purpose. Several methods have been adopted to satisfy the requirements of lowest SLL. The stationary SOUSY achieved the amplitude and density taper simultaneously by increasing the element spacing at the array periphery and by feeding the antennas with higher power at the inner positions [8]. The mobile SOUSY adopts a three-level power configuration of {1, 0.5, 0.25} to smooth the current distribution at transmitting stage and develops a Dolph–Chebychev-like distribution through an evolution strategy at receiving stage [8]. The Indian MST radar also applies the similar technique, its power distribution across the array follows an approximation of the modified Taylor weighting in both principal directions, and a large amount of T/R modules with different transmitting power are used [18]. Due to the irregular array with unchangeable transmitting power of each antenna, the PANSY adopts a phase-only synthesis on transmission and a complex synthesis of both amplitude and phase on reception, based on the simulated annealing algorithm [21].

Due to the unavoidable amplitude–phase error, element failure, interelement mutual coupling, and feeder loss, all of which will increase the SLL, we should try hard to reduce the SLL. The low SLL in the receiving stage can be effectively achieved in DBF subsystem, but the low SLL transmitting beam is hard to realize. Through trial and error, we design a "thinned" array with quantized amplitude weighting. The new calculated aperture distribution combines the effects of amplitude and density tapering and reduces the types of transmitting power as low as possible. Thus, very low SLLs can be formed in both transmitting and receiving stage.

1) Transmitting and Receiving Beam Patterns: The term "thinned" originates from [55]. In our thinned array, the antenna elements in the array are not thinned and they are also used for receiving, but the transmitted power of some elements is thinned (reduced) for better SLL. Traditional array thinning (denoted as

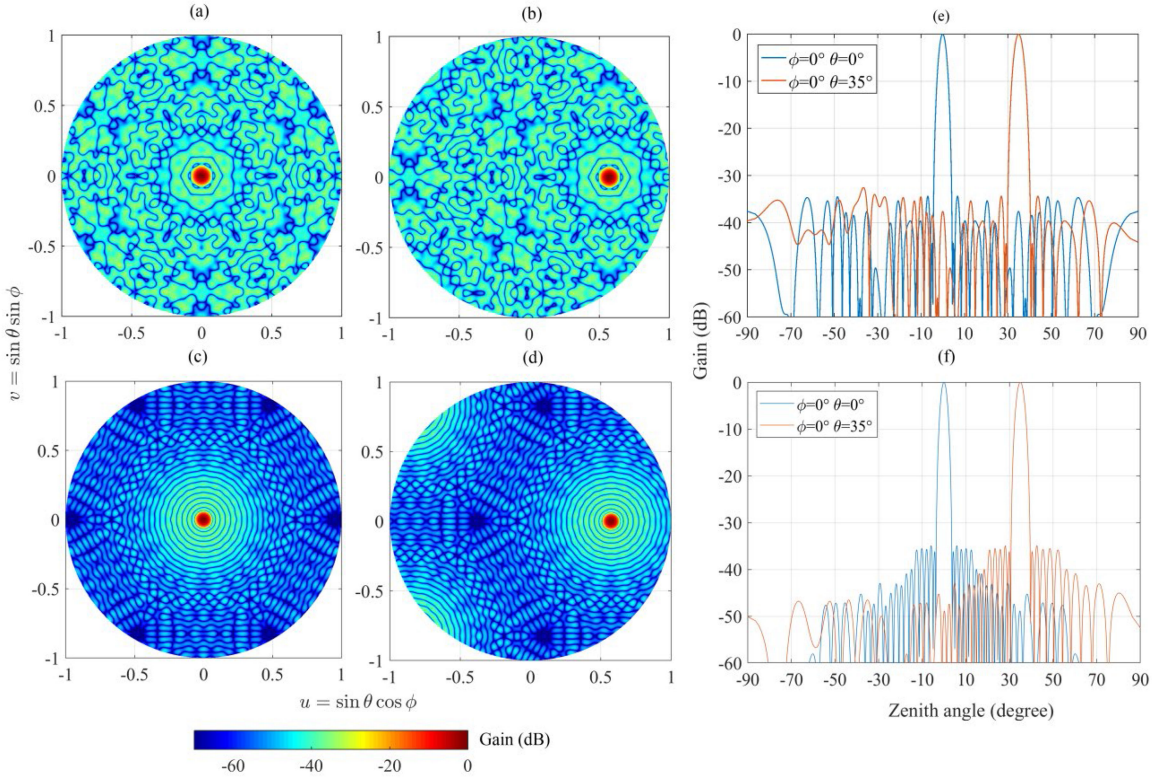

Fig. 5. Radiation patterns of the Qinzhou MST radar antenna array. The up/bottom row shows the radiation patterns of the transmitting/receiving beams. The beam zenith angle in the left/middle column is 0°/35°. The azimuth cut plots of the 2-D radiation patterns are displayed in the right column.

two-level amplitude weighting, wherein each element takes the amplitude value of zero or one regularly) has been applied to reduce cost and weight since the 1960s [62]. However, at the optimum state with the lowest SLL, almost half of the antennas of the array are unoperated [54]. Before long, this defect is improved through performing multilevel amplitude weighting. The corresponding technology has been introduced in detail in [55]. Three methods for designing multilevel amplitude weighting arrays are put forward. Method 2 is chosen by us for the array design.

After several attempts, we find that four-level amplitude weighting is adequate to generate a radiation beam with the lowest SLL close to −35 dB. The designed antenna array is displayed in Fig. 3, which is calculated by a hybrid algorithm of the combination of the method 2 in [55] and a modified iterative Fourier transform technique [56]. The four-level amplitude weighting that we use is {1, 0.5, 0.25, 0}, corresponding to the transmitting power of 2, 1, 0.5, and 0 kW, respectively. The weight 0 means that the corresponding antennas only receive, but not transmit power. Moreover, some additional modifications are applied to make the whole array illumination maintain a left right, up down, and rotational symmetric state and so ensure more symmetric radiation beams. The filling factor of the final array is near 80% and most parts of the aperture are complete.

On reception, the received signals are weighted in DBF subsystem after sampling and digital down conversion. While all elements are working in the receiving stage, the traditional circular Taylor amplitude taper [57] can be performed here to reduce the peak SLL. Fig. 5 shows the radiation patterns of the transmitting and receiving beams. The applied model taper for the receiving beams is a circular Taylor distribution with SLL = −35 dB and $\bar{n}$= 8 (number of equal amplitude sidelobes adjacent to the main beam). The lowest SLLs for the transmitting and receiving beams are −32.5 and −34.7 dB, respectively. The half-power beam width (HPBW) of the transmitting beams are 2.99° and 3.62° for the beams pointing to zenith and tilting to 35°, respectively. The corresponding parameters for the receiving beams are 2.62° and 3.22°. The directive gains are larger than 35 dB in any situations.

2) Multiple-Beam Pattern: Through dividing several isomorphic subarrays and independently controlling the radiation direction of each subarray, varied multiple-beam patterns can be formed. Fig. 6 shows two kinds of multiple-beam pattern. Excluding the black and light gray antennas, which are not powered in this mode, the antennas with different colors belong to different subarrays. If fewer beams are formed, the higher mainlobe-to-sidelobe ratio (MSR) can be gained. The three-beam pattern in Fig. 6(b) is just qualified for 3-D wind velocity observation and the seven-beam pattern in Fig. 6(d) also has relatively high MSR.

IV. Transmission and Reception

The Qinzhou MST radar will be the first full element level digital array radar among all existing MST radars. There are 997/1261 independently controllable transmitting/receiving

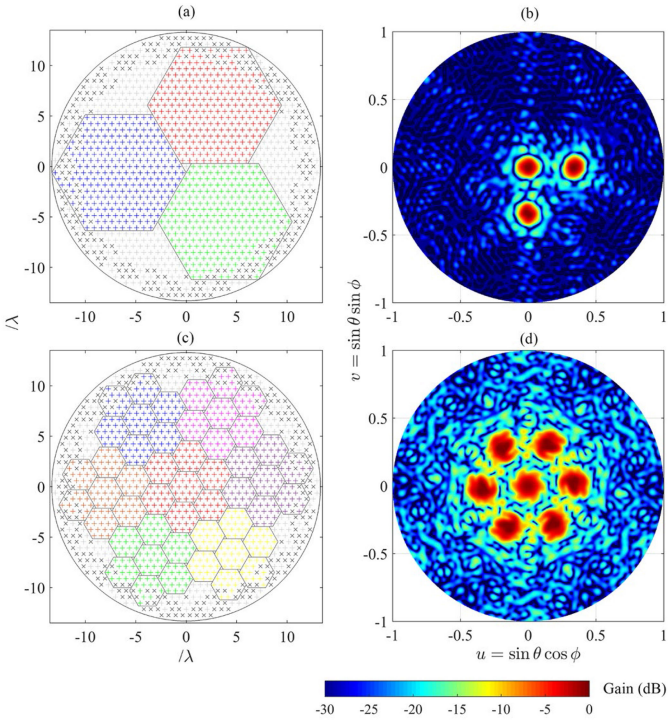

Fig. 6. Types of subarray division for multiple-beam mode with beams pointing to (a) three directions and (c) seven directions simultaneously, and the 2-D normalized radiation patterns of multiple-beam mode with the beams pointing to (b) three directions and (d) seven directions simultaneously. The specific direction of each beam for three-beam mode is (0°, 0°), (20°, 0°), and (20°, 270°). The specific direction of each beam for seven-beam mode is (0°, 0°), (20°, 4.31°), (20°, 64.31°), (20°, 124.31°), (20°, 184.31°), (20°, 244.31°), and (20°, 204.31°).

channels. The modularized structure enables the system to work in either distributed or integrated way, and so, facilitates the future remodeling and expansion.

A. T/R Module

The whole system applies a circular antenna array. There are 997 antennas connecting to T/R modules and 264 thinned antennas connecting to receiving-only (R) modules via the equilong RF cables. Six containers, uniformly distributed around the edge of the array and labeled as containers A–F, will contain all the T/R and R modules. Container A– E houses 166 T/R modules and Container F houses 167 T/R modules. Besides, each container also houses 44 R modules. Each container equips five cabinets (4 for T/R modules and 1 for R modules) and each cabinet consists of five or six (at most) crates. Each crate in the first four cabinets includes eight (at most) power amplifier modules, one digital transceiver module, one integrated control and protection module, and one monitoring module. The R modules accommodated in the remaining cabinets have no transmitting component. Before the actual mass production, the structure of the digital T/R module has been designed and the parameters are precalculated theoretically in advance. Fig. 7 shows the schematic block diagram of the eight-channel digital T/R module and Fig. 8 shows the RF front end. Currently, the prototype of the digital T/R module has been made and some core electronic components have undergone strict type selection. The eight-channel digital T/R module is connected to the DBF module via optical fiber and is also in communication with the host computer on a pulse-to-pulse basis.

In the transmitting chain, the DDS in each channel produces a low-power RF signal (15 dBm) of designative frequency and phase, which is subsequently sent to the RF front end. The low-power RF signal is first amplified to 49 dBm (80 W) through two-stage filtering and amplifying and then divided and amplified to two roads 61.5 dBm signals through two power scaleable amplifiers after a 1:2 power divider. Each Yagi feeds a high power of 60 dBm (1 kW), excluding the RF cable attenuation of about 1.5 dB, then the peak power on each crossed Yagi is 63 dBm (2 kW). Moreover, the power of each Yagi is changeable within a range of 50 dBm : 1 dB : 60 dBm by adjusting the DDS output power. The whole transmitter will operate in saturation amplification state. In the receiving chain, the tiny echo signals greater than -105 dBm are received by the Yagi and then sent to the digital transceiver module after receiving switch and multistage low noise amplifying and filtering. The receiving switch enables the users to select a receiving state. The received RF signals are directly sampled by 80 MHz analog-to-digital converter (ADC) and then sent to digital down converter (DDC) to form baseband I/Q signals. Two 6-b numerical control attenuators with an attenuation step of 0.5 dB are used between the channels to realize the 63 dB dynamic of the whole module.

B. Monitoring System

The main function of the monitoring system is the fault location and amplitude/phase calibration. Fig. 9 shows the sketch of the monitoring system. The whole monitoring system is a complete circuit. The dotted and solid lines stand for the signal flows of the transmitting and receiving states, respectively. The monitoring module provides the test signal and reference signal. When monitoring the receiving channel, the test signal is sent out from the monitoring module and injected into each receiving channel through the monitoring network. When monitoring the transmitting channel, the test signal is sent out from the tested transmitting channel and imported into the receiving channel of the monitoring module through the monitoring network. In each case, only one transmitting or receiving channel can be tested. After digitization, the monitored T/R signal and the reference signal are sent to the DBF monitoring module. Then, the processed data are transmitted to DSP, and the DSP preprocesses the test signal and transmits it to data processer. The data processer compares the test data with the standard data and then estimates the amplitude and phase errors. The receiving error data are sent to DBF module to form the echo beam together with the initial amplitude phase correction code, beam scanning code, and amplitude weighting code. The monitoring system works when the radar is off-line or in operating gap. The fault or error in any T/R module can be quickly positioned and the error will be corrected in time to ensure a long time normal operation.

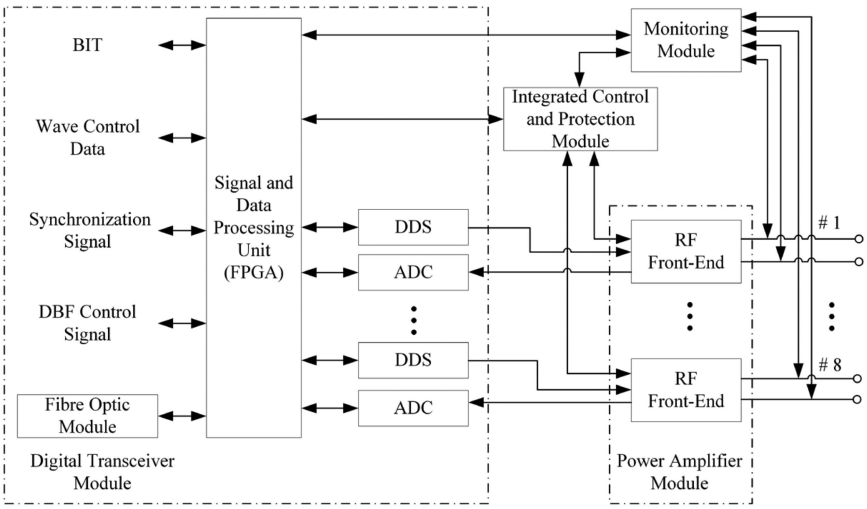

Fig. 7. Schematic block diagram of the eight-channel digital T/R module.

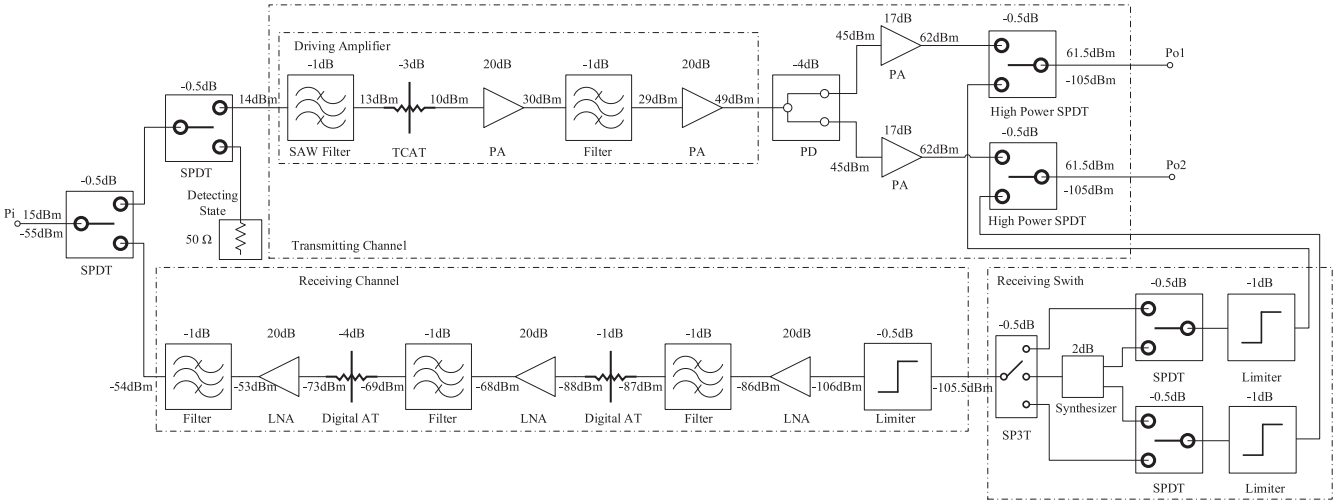

Fig. 8. Schematic block diagram of the RF front end.

C. DBF and DSP

The Qinzhou MST radar will employ at most 1261 receiving channels. In routine observation, namely, using five-beam mode (one vertical beam and four oblique beams) for 3-D wind velocity observation, all 1261 receiving signals will be complexly weighted and combined into one signal in DBF module for amplitude phase correction and SLL suppression. The circular Taylor amplitude distribution [57] will be adopted as the low SLL taper. Then, the following signal processing will be performed in a special DSP chip. The main processes include pulse compression, coherent integration, data rearranging, fast Fourier transform (FFT), and frequency-domain accumulation [51]. The processed data will be stored in the local disk and uploaded to the on-line data center. Fig. 10 displays the signal flow after the DBF processing. The future hardware for DSP will only consider the situation of routine observation mode, namely, all signals are combined into one signal. For different experiment observations, all 1261 complex signals before being transmitted to DBF module can also be exported for off-line processing. Other advanced observation techniques can be achieved using the stored multichannel data.

The Qinzhou MST radar will be a routine operation radar, and its operation modes can be switched automatically. Its pulsewidth is variable from 0.33 to 300 μs, and the allocated 4 MHz bandwidth is adequate to match the minimum chip width of 0.33 μs. The transmitting waveform can be modulated by single pulse, Barker, complementary codes, and Spano codes [52]. Pulse compression is applied to process the received signals for better range resolution and higher SNR. The coherent integration is programmable from 1 to 1024 and the spectral averaging is programmable from 1 to 128. The default number of FFT point is 512. For different velocity resolutions, it is programmable from 128 to 8192. The duty cycle can be adjusted in the range

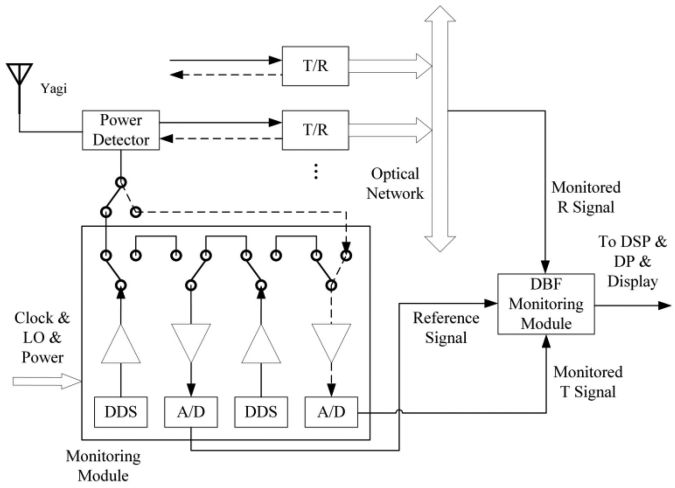

Fig. 9. Sketch of the monitoring system. The dotted lines represent the signal flows of the monitoring network under the transmitting state and the solid lines represent the signal flows of the monitoring network under the receiving state.

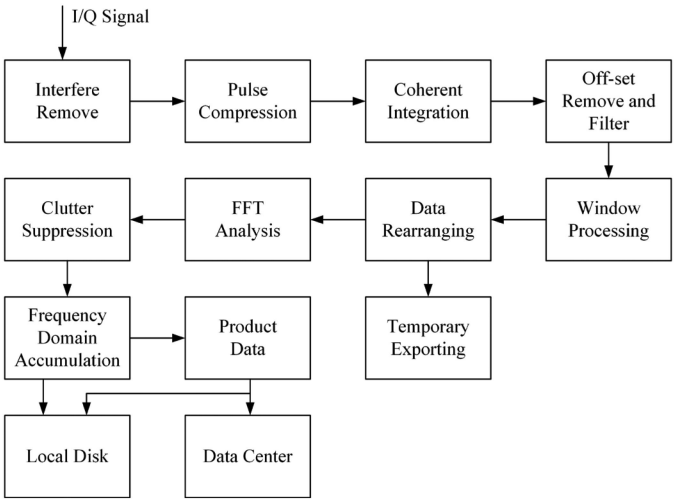

Fig. 10. Signal flow of DSP and DP.

smaller than 10% to adapt different pulse repetition intervals (PRI). The DBS mode is in common use for both atmospheric and ionospheric observations. For different detecting targets, the precalculated routine operating parameters are displayed in Table II. The ST mode is applied for troposphere and stratosphere observation and the M mode aims at the mesosphere observation. The observation for ionospheric E- and F-region irregularities is implemented in E and F modes. In the routine observation, we plan to adopt five-beam mode (four oblique beams and one vertical beam) to observe atmospheric winds and adopt seven-beam mode vertical to the local geomagnetic fields with different azimuths to observe the ionospheric irregularities. The initial beam directions refer to those of the Wuhan MST radar [14] and the HCOPAR in Fuke, Hainan [46], and can also be adjusted according to the actual observations. For other detecting experiments, these radar parameters can be flexible set.

TABLE II
SPECIFICATIONS OF THE OPERATING MODES

Aspect	ST mode	M mode	E mode	F mode
Waveform	16-bit complementary	32-bit complementary	32-bit complementary	13-bit Barker
chip width	0.5 μs	2 μs	4 μs	8 μs
PRF	3750 Hz	1250 Hz	625 Hz	154 Hz
PRI	267 μs	800 μs	1600 μs	6500 μs
duty cycle	3 %	8 %	8 %	1.6 %
NCI	64	10	2	1
NFFT	1024	1024	2048	2048
NSA	5	10	10	5
range resolution	75 m	300 m	600 m	1200 m
detecting range	2 - 30 km	60 - 100 km	80 – 200km	150–950 km
velocity range	±88 m/s	±188 m/s	±469 m/s	±230 m/s
velocity resolution	0.17 m/s	0.37 m/s	0.46 m/s	0.23 m/s
time resolution	87 s	82 s	65 s	67 s

NCI: Number of coherent integration.
NFFT: Number of FFT points.
NSA: Number of spectral average.

V. CONCLUSION

Two MST radars in Beijing and Wuhan have been developed and run in China for more than seven years with the support of the Chinese Meridian Project. They have well recorded the unique features of the midlatitude mesospheric winds over China [42]. However, the low-latitude wind observations are still lacking. With the support of the second phase of the Chinese Meridian Project, we plan to construct a new full element level digital array radar at low latitudes of China. This radar has a high requirement against surface and electromagnetic environment. It took a very long time for us to find a suitable place to place this huge system. Recently, we have just determined the construction site of the radar, Qinzhou city, Guangxi province, China. Many scientists and engineers all over the world participate in the siting and design of the Qinzhou MST radar. We have received a lot of valuable suggestions, thus the site and design of the radar have been changed and improved again and again. The final design has been determined not long ago and we have found the constructor to realize this design through an open bidding process in November 2020. This new radar is scheduled to be completed by the end of 2022. This article presents a recapitulative system design and aims at getting more helpful suggestions for the software design, construction, and operation of the new radar. The data of this radar will be open accessed and we welcome the cooperation from all over the world.

REFERENCES

[1] B. B. Balsley and K. S. Gage, "The MST radar technique: Potential for middle atmospheric studies," *Pure Appl. Geophys.*, vol. 118, no. 1, pp. 452–493, Mar. 1980.
[2] K. S. Gage and B. B. Balsley, "On the scattering and reflection mechanisms contributing to clear air radar echoes from the troposphere, stratosphere, and mesosphere," *Radio Sci.*, vol. 15, no. 2, pp. 243–257, Mar./Apr. 1980.
[3] W. K. Hocking, "A review of mesosphere–stratosphere–troposphere (MST) radar developments and studies, circa 1997–2008," *J. Atmos. Sol.-Terr. Phys.*, vol. 73, no. 9, pp. 848–882, Jun. 2011.
[4] H. G. Booker and W. E. Gordon, "Theory of radio scattering in the troposphere," *Proc. IEEE*, vol. 38, no. 4, pp. 401–412, May 1950.
[5] R. F. Woodman and A. Guillen, "Radar observations of winds and turbulence in the stratosphere and mesosphere," *J. Atmos. Sci.*, vol. 31, no. 2, pp. 493–505, Mar. 1974.

[6] B. B. Balsley, W. L. Ecklund, D. A. Carter, and P. E. Johnston, "The MST radar at Poker Flat, Alaska," *Radio Sci.*, vol. 15, no. 2, pp. 213–223, Mar. 1980.

[7] K. S. Gage and B. B. Balsley, "Doppler radar probing of the clear atmosphere," *Bull. Amer. Meteorol. Soc.*, vol. 59, no. 9, pp. 1074–1093, Aug. 1978.

[8] P. Czechowsky, G. Schmidt, and R. Rüster, "The mobile SOUSY Doppler radar: Technical design and first results," *Radio Sci.*, vol. 19, no. 1, pp. 441–450, Jan. 1984.

[9] T. E. Van Zandt, J. L. Green, K. S. Gage, and W. L. Clark, "Vertical profiles of refractivity turbulence structure constant: Comparison of observations by the sunset radar with a new theoretical model," *Radio Sci.*, vol. 13, no. 5, pp. 819–829, Sep. 1978.

[10] W. L. Ecklund, D. A. Carter, and K. S. Gage, "Sounding of the lower atmosphere with a portable 50-MHz coherent radar," *J. Geophys. Res.*, vol. 82, no. 31, pp. 4969–4971, Oct. 1977.

[11] S. Fukao, T. Sato, T. Tsuda, S. Kato, K. Wakasugi, and T. Makihira, "The MU radar with an active phased array system: 1. Antenna and power amplifiers," *Radio Sci.*, vol. 20, no. 6, pp. 1155–1168, Nov./Dec. 1985.

[12] S. Fukao, T. Tsuda, T. Sato, S. Kato, K. Wakasugi, and T. Makihira, "The MU radar with an active phased array system: 2 In-house equipment," *Radio Sci.*, vol. 20, no. 6, pp. 1169–1176, Nov./Dec. 1985.

[13] S. Fukao *et al.*, "Equatorial atmosphere radar (EAR): System description and first results," *Radio Sci.*, vol. 38, no. 3, p. 19-1–19-17, Jun. 2003.

[14] G. Chen *et al.*, "MST radars of Chinese Meridian project: System description and atmospheric wind measurement," *IEEE Trans. Geosci. Remote Sens.*, vol. 54, no. 8, pp. 4513–4523, Aug. 2016.

[15] J. Röttger *et al.*, "The Chung-Li VHF radar: Technical layout and a summary of initial results," *Radio Sci.*, vol. 25, no. 4, pp. 487–502, Jul./Aug. 1990.

[16] W. H. V. Aulock, "Properties of phased arrays," *Proc. IRE*, vol. 48, no. 10, pp. 1715–1727, Oct. 1960.

[17] X. Su and J. Li, "Analyses on utmost scan coverage of planar phased array antenna," *Modern Radar*, vol. 27, no. 7, pp. 51–53, Jul. 2005.

[18] P. B. Rao, A. R. Jain, P. Kishore, P. Balamuralidhar, S. H. Damle, and G. Viswanathan, "Indian MST radar 1. System description and sample vector wind measurements in ST mode," *Radio Sci.*, vol. 30, no. 4, pp. 1125–1138, Jul./Aug. 1995.

[19] R. Latteck *et al.*, "MAARSY: The new MST radar on Andøya—System description and first results," *Radio Sci.*, vol. 47, no. 1, Feb. 2012, Art. no. RS1006.

[20] W. K. Hocking, M. Kelley, R. Rogers, W. O. J. Brown, D. Moorcroft, and J.-P. St. Maurice, "Resolute bay VHF radar: A multipurpose tool for studies of tropospheric motions, middle atmosphere dynamics, meteor physics, and ionospheric physics," *Radio Sci.*, vol. 36, no. 6, pp. 1839–1857, Nov. 2001.

[21] K. Sato *et al.*, "Program of the Antarctic Syowa MST/IS radar (PANSY)," *J. Atmos. Sol.-Terr. Phys.*, vol. 118, Part A, pp. 2–15, Oct. 2014.

[22] D. C. Fritts and M. J. Alexander, "Correction to 'Gravity wave dynamics and effects in the middle atmosphere'," *Rev. Geophys.*, vol. 41, no. 1, Aug. 2012, Art. no. 1003.

[23] D. V. P. Kumar, K. C. Reddy, and G. Yellaiah, "MST radar observations of Perseid meteor shower 2004," *Bull. Astron. Soc. India.*, vol. 34, no. 3, pp. 281–289, Sep. 2006.

[24] F. Chen *et al.*, "Strong downdrafts preceding rapid tropopause ascent and their potential to identify cross-tropopause stratospheric intrusions," *Ann. Geophys.*, vol. 36, no. 5, pp. 1403–1417, Oct. 2018.

[25] R. M. Worthington, R. D. Palmer, and S. Fukao, "An investigation of tilted aspect-sensitive scatterers in the lower atmosphere using the MU and Aberystwyth VHF radars," *Radio Sci.*, vol. 34, no. 2, pp. 413–426, Mar. 1999.

[26] R. M. Worthington, R. D. Palmer, and S. Fukao, "Letter to the editor: Complete maps of the aspect sensitivity of VHF atmospheric radar echoes," *Ann. Geophys.*, vol. 17, no. 8, pp. 1116–1119, Aug. 1999.

[27] S. K. Dhaka, P. K. Devrajan, Y. Shibagaki, R. K. Choudhary, and S. Fukao, "Indian MST radar observations of gravity wave activities associated with tropical convection," *J. Atmos. Sol. Terr. Phys.*, vol. 63, no. 15, pp. 1631–1642, Oct. 2001.

[28] T. Sato, T. Tsuda, S. Kato, S. Morimoto, S. Fukao, and I. Kimura, "High-resolution MST observations of turbulence by using the MU radar," *Radio Sci.*, vol. 20, no. 6, pp. 1452–1460, Nov./Dec. 1985.

[29] T. Tsuda, T. Sato, K. Hirose, S. Fukao, and S. Kato, "MU radar observations of the aspect sensitivity of backscattered VHF echo power in the troposphere and lower stratosphere," *Radio Sci.*, vol. 21, no. 6, pp. 971–980, Nov. 1986.

[30] T. E. Van Zandt, "A brief history of the development of wind-profiling or MST radars," *Ann. Geophys.*, vol. 18, no. 7, pp. 740–749, Jul. 2000.

[31] W. K. Hocking *et al.*, "Detection of stratospheric ozone intrusions by windprofiler radars," *Nature*, vol. 450, pp. 281–284, Nov. 2007.

[32] A. K. Patra, P. B. Rao, V. Anandan, A. R. Jain, and G. Viswanathan, "Evidence of intermediate layer characteristics in the Gadanki radar observations of the upper E region field-aligned irregularities," *Geophys. Res. Lett.*, vol. 29, no. 14, pp. 41-1–41-4, Jul. 2002.

[33] A. K. Patra, D. V. Phanikumar, and T. K. Pant, "Gadanki radar observations of f region field-aligned irregularities during June solstice of solar minimum: First results and preliminary analysis," *J. Geophys. Res.*, vol. 114, no. A12, Dec. 2009.

[34] E. Kudeki and C. D. Fawcett, "High resolution observations of 150 km echoes at Jicamarca," *Geophys. Res. Lett.*, vol. 20, no. 18, pp. 1987–1990, Jan. 1993.

[35] M. A. Milla, E. Kudeki, P. M. Reyes, and J. L. Chau, "A multi-beam incoherent scatter radar technique for the estimation of ionospheric electron density and T_e/T_i profiles at Jicamarca," *J. Atmos. Sol.-Terr. Phys.*, vol. 105/106, pp. 214–229, Dec. 2013.

[36] M. Yamamoto and S. Fukao, "Mid-latitude E region field-aligned irregularities observed with the MU radar," *J. Geophys. Res.*, vol. 96, no. A9, pp. 15943–15949, Sep. 1991.

[37] S. Fukao, Y. Ozawa, T. Yokoyama, M. Yamamoto, and R. T. Tsunoda, "First observations of the spatial structure of F region 3-m-scale field-aligned irregularities with the equatorial atmosphere radar in Indonesia," *J. Geophys. Res.*, vol. 109, no. A2, Feb. 2004.

[38] S. Fukao, J. P. Mcclure, A. Ito, T. Sato, I. Kimura, and T. Tsuda, "First VHF radar observation of midlatitude F-region field-aligned irregularities," *Geophys. Res. Lett.*, vol. 15, no. 8, pp. 768–771, Jan. 1988.

[39] T. Sato *et al.*, "Ionospheric incoherent scatter measurements with the middle and upper atmosphere radar: Techniques and capability," *Radio Sci.*, vol. 24, no. 1, pp. 85–98, Jan./Feb. 1989.

[40] C. Wang, "New chains of space weather monitoring stations in china," *Space Weather*, vol. 8, no. 8, Aug. 2010.

[41] C. Wang, "Development of the Chinese meridian project," *Chin. J. Space. Sci.*, vol. 30, no. 4, pp. 382–384, Aug. 2010.

[42] W. F. Zhang *et al.*, "Statistical study of the midlatitude mesospheric vertical winds observed by the Wuhan and Beijing MST radars in China," *J. Geophys. Res., Atmos.*, vol. 125, no. 18, Aug. 2020.

[43] G. Chen *et al.*, "Low latitude daytime F region irregularities observed in two geomagnetically quiet days by the Hainan coherent scatter phased array radar (HCOPAR)," *J. Geophys. Res. Space Phys.*, vol. 122, no. 2, pp. 2645–2654, Feb. 2017.

[44] T. Renkwitz, W. Singer, R. Latteck, and M. Rapp, "Multi beam observations of cosmic radio noise using a VHF radar with beam forming by a butler matrix," *Adv. Radio Sci.*, vol. 9, no. 26, pp. 349–357, Aug. 2011.

[45] E. Kudeki and G. R. Stitt, "Frequency domain interferometry: A high resolution radar technique for studies of atmospheric turbulence," *Geophys. Res. Lett.*, vol. 14, no. 3, pp. 198–201, Jan. 1987.

[46] G. Chen *et al.*, "Hainan coherent scatter phased array radar (HCOPAR): System design and ionospheric irregularity observations," *IEEE Trans. Geosci. Remote Sens.*, vol. 55, no. 8, pp. 4757–4765, Aug. 2017.

[47] D. T. Farley, H. M. Ierkic, and B. G. Fejer, "Radar interferometry—A new technique for studying plasma turbulence in the ionosphere," *J. Geophys. Res.*, vol. 86, no. A3, pp. 1467–1472, Mar. 1981.

[48] J. Chen, C. Wang, Y. Chu, C. Su, and H. Hashiguchi, "3-D radar imaging of E-region field-aligned plasma irregularities by using multireceiver and multifrequency techniques," *IEEE Trans. Geosci. Remote Sens.*, vol. 56, no. 10, pp. 5591–5599, Oct. 2018.

[49] Y. H. Chu and K. F. Yang, "Reconstruction of spatial structure of thin layer in sporadic e region by using VHF coherent scatter radar," *Radio Sci.*, vol. 44, no. 5, Sep. 2009, Art. no. RS5003.

[50] W. K. Hocking, "System design, signal-processing procedures, and preliminary results for the Canadian (London, Ontario) VHF atmospheric radar," *Radio Sci.*, vol. 32, no. 2, pp. 687–706, Mar. 1997.

[51] S. R. Thatiparthi, R. R. Gudheti, and V. Sourirajan, "MST radar signal processing using wavelet-based denoising," *IEEE Geosci. Remote Sens. Lett.*, vol. 6, no. 4, pp. 752–756, Oct. 2009.

[52] E. Spano and O. Ghebrebrhan, "Pulse coding techniques for ST/MST radar systems: A general approach based on a matrix formulation," *IEEE Trans. Geosci. Remote Sens.*, vol. 34, no. 2, pp. 304–316, Mar. 1996.

[53] K. Wakasugi and S. Fukao, "Sidelobe properties of a complementary code used in MST radar observations," *IEEE Trans. Geosci. Remote Sens.*, vol. GE-23, no. 1, pp. 57–59, Feb. 1985.

[54] W. P. M. N. Keizer, "Amplitude-only low sidelobe synthesis for large thinned circular array antennas," *IEEE Trans. Antennas Propag.*, vol. 60, no. 2, pp. 1157–1161, Feb. 2012.
[55] R. J. Mailloux and E. Cohen, "Statistically thinned arrays with quantized element weights," *IEEE Trans. Antennas Propag.*, vol. 39, no. 4, pp. 436–447, Apr. 1991.
[56] X. Wang, Y. Jiao, and Y. Tan, "Synthesis of large thinned planar arrays using a modified iterative Fourier technique," *IEEE Trans. Antennas Propag.*, vol. 62, no. 4, pp. 1564–1571, Apr. 2014.
[57] T. Taylor, "Design of circular apertures for narrow beamwidth and low sidelobes," *IRE Trans. Antennas Propag.*, vol. 8, no. 1, pp. 17–22, Jan. 1960.
[58] J. S. Chen, "On the phase biases of multiple-frequency radar returns of mesosphere-stratosphere-troposphere radar," *Radio Sci.*, vol. 39, no. 5, Oct. 2004.
[59] G. Stober *et al.*, "MAARSY- the new MST radar on Andøya: First results of spaced antenna and Doppler measurements of atmospheric winds in the troposphere and mesosphere using a partial array," *Adv. Radio Sci.*, vol. 10, pp. 291–298, 2012.
[60] H. Luce *et al.*, "A frequency radar interferometric imaging applied with high resolution methods," *J. Atmos. Sol.-Terr. Phys.*, vol. 63, pp. 221–234, 2001.
[61] J. Jones, A. R. Webster, and W. K. Hocking, "An improved interferometer design for use with meteor radars," *Radio Sci.*, vol. 33, no. 1, pp. 55–65, Jan./Feb. 1998.
[62] M. Skolnik, J. Sherman, and F. Ogg, "Statistically designed density-tapered arrays," *IEEE Trans. Antennas Propag.*, vol. 12, no. 4, pp. 408–417, Jul. 1964.

Gang Chen was born in Wuhan, China, in 1980. He received the B.S. degree in electronic engineering and the Ph.D. degree in space physics from Wuhan University, Wuhan, China, in 2002 and 2007, respectively.

From 2009 to 2011, he was an Assistant Professor with the Electronic Information School, Wuhan University, where he has been a Professor with the Department of Space Physics, School of Electronic Information, since 2012. His research interests include ionospheric and atmospheric physics, as well as remote sensing technology for the disturbances in the ionosphere and atmosphere.

Zhiqiu He was born in Wuhan, China, in 1993. He received the B.S. degree in communication engineering from Jianghan University, Wuhan, China, in 2016. He is currently working toward the Ph.D. degree in space exploration and information processing technology with the School of Electronic Information, Wuhan University, Wuhan, China.

His research interests include synthesis of array antennas, radar signal processing, and radar system design.

Shaodong Zhang was born in Hubei, China, in 1972. He received the B.S. degree from the Department of Space Physics, Wuhan University, Wuhan, China, in 1993, and the master's and Ph.D. degrees in space physics from the Wuhan Institute of Physics and Mathematics, Chinese Academy of Sciences, Wuhan, China, in 1995 and 1998, respectively.

From 2000 to 2003, he was an Assistant Professor with the Electronic Information School, Wuhan University, where he has been a Professor with the Space Physics Department, since 2003 and is currently the Director of the Chinese Meridian Space Weather Monitoring Project. He was constituted as the President of the Electronic Information School, in 2009 and transferred to be the Head of the Department of Undergraduate Education, Wuhan University.

Brian Fuller was born in South Australia, in 1956. He received the B.S. degree in computer science from the University of Adelaide, Adelaide, SA, Australia, in 1987, and the Certificate in Japanese from Vocational Language Learning Center, Adelaide, SA, Australia, in 2004.

From 1974 to 1989, he was full-time employed with the Department of Physics, University of Adelaide, working on the development and production of electronic equipment. From 1989 to 1992, he was part-time employed with the Department of Physics, University of Adelaide, focusing on the design of radar data acquisition hardware and software, and in 1987, established Genesis Software Pty Ltd., using the remainder of the time. Since then, he developed the new-generation radar data acquisition system, which has been integrated into more than 60 atmospheric radar systems installed worldwide. From 2008 to 2011, he successfully led the development of an MST-class VHF radar. In recent years, he has been studying on the development of frequency and time synchronized radar stations for meteor orbits determination and forward scatter meteor observations.

Wanlin Gong received the B.S. degree in electronic information science and technology and the Ph.D. degree in space physics from the School of Electronic Information, Wuhan University, Wuhan, China, in 2012 and 2019, respectively.

From 2012 to 2014, he was a Hardware Engineer with Guangzhou South Mapping Instrument Company Ltd., Guangzhou, China. He is currently an Assistant Professor with the Innovation Practice Center for College Students, Wuhan University. His research interests include the research of space exploration and information processing technology.

Guotao Yang received the Ph.D. degree from the Wuhan Institute of Physics and Mathematics, Chinese Academy of Sciences, Wuhan, China, in 2004.

He was a Postdoctoral Researcher with the Instituto Nacional de Pesquisas Espaciais, São José dos Campos, Brazil. He was elected in the Hundred Talents Program of the Chinese Academy of Sciences, Beijing, China, in 2009. He is currently a Research Scientist with the National Space Science Center, Chinese Academy of Science.

Weifan Zhang received the B.S. degree in electronic information science and technology in 2016 from Wuhan University, Wuhan, China, where she is currently working toward the Ph.D. degree in space physics with the Electronic Information School.

Her research interests include radar signal processing and atmospheric physics.